47th AIAA Aerospace Sciences Meeting Including The New Horizons Forum and Aerospace Exposition
5 - 8 January 2009, Orlando, Florida
AIAA 2009-853

Mean Flow – Acoustic Correlations for Dual-Stream Asymmetric Jets

Preben E. Nielsen* and Dimitri Papamoschou†
University of California, Irvine, CA 92697, USA

We present an experimental study, comprising acoustic and mean-flow measurements, of several fan-flow deflector configurations in a subscale dual-stream supersonic turbofan nozzle. The deflectors encompassed internal vanes and external wedges. The aim of the study was to investigate trends of high-frequency noise reduction, in the direction of peak emission, versus the distortion of the velocity field in the jet plume. The distortion is quantified in terms of the volume of the inflectional region of the jet, in a particular azimuthal direction, normalized by the volume of the high-speed region of the jet. It is observed that fan flow deflection generally increases the volume of the inflectional region (in the downward and sideline azimuthal directions) and decreases the volume of the high-speed region. Correlations of sound pressure level with the volume-ratio parameter show rapid noise suppression for small values of the volume ratio followed by slower noise reduction at higher values. The correlations appear to validate the hypothesized physics of noise suppression by an enlarged secondary core, and provide practical guidance for the implementation of the fan flow deflection method

Nomenclature

A	= nozzle exit area
BPR	= bypass ratio
D_f	= nozzle fan diameter
f	= frequency
M	= Mach number
NPR	= nozzle pressure ratio
r	= radial direction
Sr	= Strouhal number = $f D_f / U_s$
U	= nozzle exit velocity
u	= mean axial velocity in jet plume
$\mathcal{V}$	= volume
x	= axial direction (from plug tip)
y	= vertical transverse direction
z	= horizontal transverse direction
θ	= polar angle from jet axis
ϕ	= azimuth angle from downward vertical

Subscripts

FS	= full-scale
p	= primary (core) exhaust
PC	= primary core
s	= secondary (fan) exhaust
SC	= secondary core

* Graduate Student Researcher, Department of Mechanical and Aerospace Engineering, nielsenp@uci.edu, AIAA Student Member.
† Professor, Department of Mechanical and Aerospace Engineering, dpapamos@uci.edu, AIAA Fellow.

I. Introduction

The use of asymmetric dual-stream jets for the exhaust of turbofan engines has demonstrated the potential for noise in reduction in subsonic and supersonic applications[1-3]. The purpose of this study is to further understand and model the connection between the distortion of the mean flow field and the resulting directional noise suppression. The study focuses on supersonic turbofan exhaust but the findings are expected to be general enough to be applicable to subsonic flows as well. The asymmetry of the plume is created by the use of fan flow deflectors (FFD) as depicted in Fig. 1.

Past work has focused on correlating the overall sound pressure level (OASPL) with the mean velocity gradient[4]. The rationale was that the rate of production of turbulent kinetic energy (TKE) is driven by the velocity gradient, therefore reductions in the gradient should result in less TKE and thus less potential for noise emission in the direction of the reduced gradients. The connection between TKE and sound generation is evident in acoustic-analogy models used for noise prediction[5]. Tentative correlations were obtained between the reduction in OASPL and the reduction of the velocity gradient near the end of the primary potential core[4]. That study did not examine the effects of the inflectional layers of the jet, to be defined below, that occur in the vicinity of the jet exit. While the OASPL is dominated by low-frequency sound emitted from near the end of the potential core, turbulence in the vicinity of the nozzle exit emits high-frequency sound that at full scale is relevant to noise perceived by humans. It is thus important to try to model the changes in sound emission from the initial region of the shear layer as the jet is distorted from a coaxial state to an asymmetric state.

The discussion that follows is based on the work by Papamoschou[1] and parallels the coaxial jet model by Fisher and Preston[6], with minor variations in the definitions of regions. Referring to Fig. 2(a), there is a high-velocity region that contains the strongest noise sources, called here the "primary core" (PC). One can define the primary core based on a velocity threshold, e.g., $u/U_p \geq 0.8$. To describe the extent of the secondary flow, one can consider a secondary potential core but its definition, based on a velocity criterion, is ambiguous. Instead, we define a "secondary core" (SC) based on the inflection points of the radial velocity distribution. The initial region of the jet is characterized by three inflection points: *i1*, *i2*, and *i3*, as seen in Fig. 2(a). The first inflection point, *i1*, defines approximately the dividing streamline of the primary (inner) shear layer and the third inflection point, *i3*, is nearly coincident with the dividing streamline of the secondary (outer) shear layer. Dahl and Morris[7], in their mean-flow model for coaxial jets, used basically the same criterion to distinguish the two shear layers. Past the initial region, the outer inflection points disappear and the profile reduces to that of a single-stream jet. The downstream distance where the number of inflection points reduces from three to one marks the end of the secondary core.

Fisher and Preston[6] determined that, for velocity ratios typical of turbofan engines ($U_s/U_p \sim 0.7$), the primary shear layer covered by the secondary core is practically silent. This observation is highly pertinent to the attempts to reduce noise by concentrating low-speed fan flow on the underside of the jet. Extending the secondary core, relative to the primary core, silences a larger portion of the inner shear layer. In this work we seek to establish correlations between the distortion of the mean flow field and the noise reduction. Acoustic measurements, mean flow surveys, and noise source maps are used to build correlations that provide insight into the physics of noise suppression and help with the optimization of asymmetry-inducing schemes such as fan flow deflectors.

II. Experimental Details

A. Nozzle and Flow Conditions

The nozzle design in this study is based on the NASA GRC 3BB separate-flow nozzle, nominally for bypass ratio BPR = 5. The fan duct was reduced in diameter to produce BPR = 2.7 at the conditions specified by the engine cycle analysis given by the "Acoustic Tests" column of Table 1, and the entire nozzle was scaled down by factor of eight to fit within the flow rate capability of the UCI facility. The Reynolds number of the jet, based on fan diameter, was 0.92×10^6 in the acoustic tests and 0.47×10^6 in the mean velocity surveys. The nozzle construction and coordinates of the nozzle are shown in Fig. 3. The baseline nozzles were fabricated using a rapid prototyping epoxy method. The fan exit diameter was $D_f = 28.1$ mm, and the fan exit height was 1.8 mm.

Fan flow deflection is achieved through the use of internal airfoil-shaped vanes and external wedges, as depicted in Fig. 4. The small fan exit height necessitated the fabrication of vanes of very small dimensions, of the same order as the fan exit height. The vanes were micro-machined from high-strength polycarbonate material using CAD/CAM facilities at U.C. Irvine (Roland MDX-40 Subtractive Rapid Prototyping Milling machine). Refinements in the manufacturing method of the vanes have lead to a higher accuracy product than previous studies. The vane cross

sections encompassed asymmetric airfoils with NACA 4412 and 7514 cross sections. The base and tip of each vane are shaped to conform to the geometry of the fan and core ducts at the exact location where the vane is attached. The vane chord length was 3 mm and the vane trailing edge was situated 2 mm upstream of the nozzle exit. Using one-dimensional theory it is estimated that the Mach numbers at the leading and trailing edges of the vane were 0.4 and 0.8, respectively. Nozzles were tested with both single-pair (2V) and two-pair (4V) vane configurations at various azimuth angles and angles of attack. The wedges used were both solid and perforated and were tested at a various axial positions downstream of the fan exit. The perforated wedges were constructed of metal mesh with porosity of 50% and mesh size of 1 mm. Perforated wedges (or flaps) allow some velocity at the base of the wedge, thus prevent strong velocity gradients that have been shown to cause significant localized noise[8]. Table 2 lists the geometric parameters of the deflectors and sample results to be discussed later. Figure 5 shows photos of some the deflectors tested.

B. Aeroacoustic testing

Aeroacoustic tests were conducted in U.C. Irvine's Jet Aeroacoustics Facility, depicted in Fig. 6. This is a subscale facility (approximately 1/50th of full scale for the tests in question) that uses helium-air mixtures for simulating the exhaust velocity and density of hot jets. In these tests, the exhaust conditions of the BPR=2.7 cycle were matched. Jet noise was recorded by a microphone array consisting of eight 3.2 mm condenser microphones (Bruel & Kjaer, Model 4138) arranged on a circular arc centered at the vicinity of the nozzle exit. The polar aperture of the array is 30° and the array radius is 1 m. The entire array structure was rotated around its center to place the array at the desired polar angle. Variations of the azimuth angle are possible by rotating the nozzle. This study encompassed the azimuth angles ϕ=0° (downward) and 60° (sideline). The arrangement of the microphones inside the anechoic chamber, and the principal electronic components, are shown in Fig. 6. Data from the microphone array were processed into lossless narrowband sound pressure level (SPL) spectra and overall sound pressure level (OASPL). Estimates of Effective Perceived Noise Level were (EPNL) were obtained using the procedure of Ref. 1. The EPNL was evaluated for a constant-altitude flyover (1500-ft altitude) in the downward (φ_{mic} = 0°) and sideline (φ_{mic} = 60°) directions. In this report the PNL and EPNL are based on an engine thrust of 120 kN, flyover Mach number of 0.25, and engine angle of attack of 10°. SPL spectra at full-scale size are presented by dividing the laboratory frequencies by the scale factor of 50 and are referenced to a distance of r/D_f =100 from the jet nozzle exit. The sound intensity can also be discretized into 1/3-octave bands for full scale frequencies which can also be used to determine the acoustic performance of the various fan flow deflection configurations. We present results for the 18th and 21st 1/3-octave bands (f = 500 Hz, Sr = 1.16; f = 1000 Hz, Sr = 2.32) which are very critical to human perception of noise. The microphone array enabled noise source localization discussed in Section III.B.

C. Mean Velocity Surveys

Each acoustic test was followed by a mean velocity survey in a duplicate dual-stream apparatus. Due to large run times, pure air was used in both primary and secondary streams instead of the helium/air mixtures. Therefore, the flow velocities were lower than those in the acoustic tests. However, the velocity ratio and primary Mach number were held the same as in the acoustic tests. The mean axial velocity in the jet plume was surveyed using a Pitot rake system consisting of five probes, spaced apart by 10 mm, with hypodermic 0.5-mm internal diameter tips as shown in Fig. 7. The small diameter of the Pitot probe tips facilitated the study of the subtle inflectional layers in the near field of the jet. Each probe is connected individually to a Setra Model 207 pressure transducer. Mounted on a three-dimensional motorized traverse, the rake translated along a pre-programmed path consisting of 28 axial (x) planes spaced apart by 12.7 mm. On each axial plane, the rake swept the jet flow along a reciprocating pattern in y, the z-position being incremented by 1 mm after each y-stroke. This pattern is illustrated by the dashed line of Fig.7. The speed of the y-movement, 5 mm/s, was selected carefully after evaluating the time-response of the Pitot rake system by traversing at different speeds and ensuring that the details of the velocity profile matched those measured when traversing at very low speed.

The pressure measurements on each axial plane were interpolated on a fixed y-z grid. Mach number and velocity fields were computed from the Pitot measurements under the assumptions of constant static pressure (equal to ambient pressure) and constant total temperature (equal to room temperature). Smoothing of the velocity profiles and computation of the velocity gradients was performed using a Savitzky-Golay filter.

For each axial station, the radial derivatives were calculated on the radial-azimuthal ($r - \varphi$) coordinate system The origin of the ($r - \varphi$) system was defined as the centroid of the region where the Pitot pressure exceeds 95% of its maximum value. The first and second derivatives were calculated along radial lines from φ=0 to 358° in

increments of 2°. Calculation of second derivatives requires great care in selecting the filter sizes used in the smoothing and differentiation of the velocity profiles. Here an adaptive filter size was used, ranging from 0.013 D_f in the high-speed region to 0.08 D_f in the low-speed region of the jet.

III. Results

A. Single-microphone acoustics

In this section we discuss acoustics that did not involve correlations between the array microphones. First we present "acoustic summaries" of selected cases comprising the following quantities: narrowband sound pressure level (SPL) lossless spectra, scaled to full-scale frequency (scale factor of 50), at selected polar angles; directivity of OASPL; PNL versus flyover time; PNL versus observer polar angle; and estimate of EPNL. These quantities are compared against their respective baseline values (red curves).

The acoustic summaries for cases $4V_a$ and W_c are shown in Fig.8. Both of these cases are quite effective in reducing the downward EPNL. For Case $4V_a$ we observe deep reductions in the spectral levels at low polar angles, followed by a mild increase at high polar angles. The perforated wedge case W_c produces a more moderate noise reduction at low polar angles but without significant increase at large polar angles.

Important insight into the physics of noise reduction is gained by examining the spectra at low polar angle, in this case θ=30 deg. It is instructive to compare the FFD cases not only with the baseline jet but also with the core-alone and fan-alone jets. The fan-alone and core-alone cases may be viewed as the upper and lower bounds, respectively, of noise production of a specific jet. Referring to Fig.2, if the inflectional layers vanish we are left with the core jet; of they become very long relative to the primary core, we expect the noise emission to approach that of the fan-alone case.

Such comparisons are made in Fig.9 for cases $4V_a$ and W_c. First we observe that the core-alone jet is the noisiest of all the flows, even though its thrust is 35% of the full jet and 55% of the fan-alone case. Adding the fan stream in a symmetric fashion (baseline) reduces sound for f_{FS} > 500 Hz and increases sound for lower frequencies. The reduction in high-frequency noise is related to the "shielding" effect of the inflectional layer of the secondary flow that we discussed in the introduction. It is this effect that we are trying to augment here by enlarging the inflectional layer on the underside of the jet. The increase in low-frequency sound has to do with the increase in the volume of the fully-mixed jet past the end of the primary potential core. It is remarkable that addition of the secondary (fan) flow results in a quieter jet in terms of perceived noise, even though the thrust is increased three-fold. If we scaled the results to equal thrust the noise reduction would be even more dramatic, but doing so may complicate the physical arguments.

Deflection of the fan flow results in significant reduction of the spectral levels. Fig.9a shows that for f_{FS} > 750 Hz, the spectrum of case $4V_a$ practically coincides with that of the fan-alone jet. For the perforated wedge case W_c (Fig.9b) the spectrum coincides with the fan-alone spectrum for f_{FS} > 1000 Hz. Generally the fan flow deflection is very effective in reducing noise levels for frequencies above 100 Hz full-scale, which are relevant to aircraft noise. To understand and model these noise reductions, we need to focus in the region of the flow that emits high-frequency noise. As will be shown in the next section, this region is very close to the nozzle exit.

B. Noise source maps

Cross-correlations of the microphone signals enabled the determination of an axial noise source distribution. The source imaging procedure follows the general deconvolution approach of Brooks and Humphries[9] but differs in the inversion algorithm and in the formulation of a directional source[10]. The imaging procedure produces a self-consistent source distribution, that is, its axial integration (weighted by the distance factor) gives the autospectrum of the far-field pressure for each polar angle surveyed. Figure 10 shows contour maps of the deconvolved noise source and plots of the peak noise source location for the baseline, $4V_a$, and W_c jets. For the baseline jet, the maximum level of the noise source is located at x/D_f=6 and f_{FS} = 100 Hz (Sr=0.23). Cases $4V_a$ and W_c show significant decrease in the noise source levels, with the maximum noise coming from x/D_f=4 and f_{FS} = 100 Hz. In other words, the fan flow deflectors resulted in both contraction and attenuation of the noise source for all frequencies. It is noteworthy that the maximum noise level (at 100 Hz full scale) is of marginal importance to aircraft noise. As shown by the plots of peak noise source location, emission of great impact to aircraft noise (f_{FS} > 500 Hz) comes from approximately 0 to 2 fan diameters downstream of the plug tip. The location of peak noise seen in the noise source maps is consistent with the termination of the primary core of the jet to be discussed in the following section.

C. Mean velocity

In this section we discuss flow field data pertaining to the distribution of the axial mean velocity and its second radial derivative. Referring to Figs. 11-13, the velocity data are presented as a composite of isocontours on the symmetry (x-y) plane and a number of transverse (y-z) planes, as well as line plots on the symmetry plane. The second-derivative data are shown in terms of the locus of the inflectional layer *i2-i3* on the symmetry plane and on various transverse planes (green regions), and radial plots of the second-derivative distribution on the symmetry plane. The inflectional-layer maps include the extent of the high-speed region of the jet (red).

For the baseline case, Fig. 11, we obtain a fairly axisymmetric distribution of the velocity field and its inflectional layer. The primary potential core, defined as $u/U_p \geq 0.8$, extends to x/D_f=6.3. The inflectional layer dissipates quickly past x/D_f=1.5. For the vane case $4V_a$, Fig. 12, we have a substantial thickening of the flow on the underside of the jet and an attendant elongation of the downward inflectional layer to $x/D_f \approx 5$. The primary potential core is contracted to x/D_f=5.2. The wedge case W_c distorts the flow in more subtle ways, as shown in Fig.13. The cross-sectional profile becomes "pear-shaped" and the downward inflectional layer slightly elongated and thickened mainly in the sideline direction. The primary potential core is contracted to x/D_f=5.6. We observe that in both vane and wedge cases, the inflectional layer appears more substantial (in thickness and axial extent) than in the baseline case. This is characteristic of all the FFD cases examined in this study. Also, in all cases the primary potential core was contracted by various amounts.

D. Flow-acoustic correlations

Our goal is to establish correlations between the distortion of the mean flow and the change in its peak noise emission. This could be considered as a simplistic exercise as it omits the crucial intermediate step of the alteration in the turbulence structure and its statistics, which we are unable to measure. Our model is based on the observation stated in the introduction, i.e., that the inflectional layer *i2-i3* silences the core flow that it envelops. We realize that an exact relation between noise level and extent of the inflectional layer could be an overly optimistic expectation given the complexity of the turbulence field. We hope instead to obtain a trend that will validate the basic physics and provide guidance for effective implementation of the FFD method.

The correlation parameter should describe the extent of the inflectional layer (secondary core), at a given azimuthal direction, relative to the high-speed region it encloses. The length alone of the secondary core may not be sufficient as we observe significant variations in the secondary-core thickness at a given axial station. Therefore, we choose to examine the volume of the secondary core as a fraction of the volume of the high-speed region. Figure 14 illustrates the inflectional areas used in the calculation of the volume. For the downward emission we used the sector $-30^o \leq \phi \leq 30^o$; and for the sideline direction, the average of the sectors $-90^o \leq \phi < -30^o$ and $30^o < \phi \leq 90^o$. The evolution of the downward inflectional area with axial distance is exemplified in Fig. 15 for the baseline jet and jet $2V_b$. For all the cases examined here, the area of the secondary core goes to zero at specific values of x. This makes the volume of the secondary core, $\mathcal{V}_{SC}$, a fairly robust measure of the extent of the inflectional region of the jet. The volume of the primary core, $\mathcal{V}_{PC}$, is defined here as the volume of the flow with $u/U_p \geq 0.8$. We use the ratio $\mathcal{V}_{SC}/\mathcal{V}_{PC}$ as our noise correlation parameter.

As mentioned in the introduction, we are interested in sound emission that has strong relevance to perceived aircraft noise. To this end, we examine the 1/3-octave noise levels for bands 18 (500 Hz full-scale, Sr=1.16) and 21 (1000 Hz full-scale, Sr=2.32) at polar angles θ=30 and 40 deg, i.e., around the direction of peak emission. Figure 16 plots correlations of these noise levels versus the volume ratio $\mathcal{V}_{SC}/\mathcal{V}_{PC}$. Table 2 lists the results for the 18th 1/3-octave band at θ=30 deg. Included in the graphs are the cases of the core-alone and fan-alone jets. Although there is significant scatter, a trend of noise reduction versus $\mathcal{V}_{SC}/\mathcal{V}_{PC}$ is evident in all the graphs. The trend is rapid for small values of $\mathcal{V}_{SC}/\mathcal{V}_{PC}$ and flattens out for large values of $\mathcal{V}_{SC}/\mathcal{V}_{PC}$. For $\mathcal{V}_{SC}/\mathcal{V}_{PC}$ roughly exceeding 0.15, the noise becomes close to, or slightly less than, the noise of the fan-alone jet. This is consistent with our expectation that a large secondary core effectively silences sound emission from the primary core in the direction of peak emission. Outlier cases with noise reduction considerably larger than that obtained by a rough trend line through the data involve wedge deflectors. This suggests that the deflection using wedges involves fluid dynamical effects that may not be captured by the simple volume-based correlation parameter used here.

IV. Conclusions

We have conducted an experimental study, comprising acoustic and mean-flow measurements, of several fan-flow deflector configurations in a subscale dual-stream supersonic turbofan nozzle. The aim of the study was to investigate trends of noise reduction versus the distortion of the velocity field in the jet plume. The distortion is quantified in terms of the volume of the inflectional region (secondary core) of the jet, in a particular azimuthal direction, normalized by the volume of the high-speed (primary core) region of the jet. Noise reduction is quantified as the reduction in 1/3-octave levels in bands 18 and 21 (500 Hz and 1000 Hz full-scale frequency) in the direction of peak emission. As a general observation, fan flow deflection increases the volume of the secondary core (in the downward and sideline azimuthal directions) and decreases the volume of the high-speed region. In other words, the physics of noise reduction apparently involve "shielding" of the high-speed noise sources by an enlarged secondary core in combination with the compaction of those noise sources.

Correlation of sound pressure level with the volume-ratio parameter shows a hyperbolic-tangent-like trend, with rapid noise suppression for small values of the volume ratio followed by slower noise reduction at higher values. The "asymptote" of the trend is the noise of the fan flow alone, but in some cases the jet becomes slightly quieter than the fan-alone limit. Although the correlations have significant scatter, they appear to validate the hypothesized physics of noise suppression by an enlarged secondary core. In addition, the correlations provide guidance in practical application and prediction of the fan flow deflection method. For the particular nozzle used here, a volume ratio above 0.15 does not offer any additional benefit in the reduction of peak noise emission; however, it may aggravate noise emitted in the 90-deg direction because of the large turning effort and attendant self-noise of the deflectors. The aerodynamic penalty of large deflections should also be taken into account. A preliminary guidance is that a volume ratio in the neighborhood of 0.1 may be optimal for effective noise reduction.

Acknowledgment

We acknowledge the support by NASA Cooperative Agreement NNX07AC62A, monitored by Dr. Khairul Zaman.

References

[1]Papamoschou, D., "Fan Flow Deflection in Simulated Turbofan Exhaust," *AIAA Journal*, Vol. 44, No.12, 2006, pp. 3088-3097.

[2]Zaman, K., Bridges, J., and Papamoschou, D., "Offset Stream Technology - Comparison of Results from UCI and GRC," AIAA-2007-0438, Jan. 2007.

[3]Papamoschou, D., and Nielsen, P., "Fan Flow Deflection for Supersonic Turbofan Engines," AIAA Paper 2008-0039, Jan. 2008.

[4]Nielsen, P., and Papamoschou, D., "Optimization of Fan Flow Deflection for Supersonic Turbofan Engines," AIAA Paper 2008-3061, May 2008.

[5]Birch, S.F., Lyubimov, D.A., Maslov, V.P., and Secundov, A.N., "Noise Prediction for Chevron Nozzle Flows," AIAA Paper 2006-2600, May 2006.

[6]Fisher, M.J., and Preston, G.A., "A Modelling of the Noise from Simple Coaxial Jets, Part I: With Unheated Primary Flow," *Journal of Sound and Vibration*, Vol., 209, No.3, pp. 385-403, 1998.

[7]Dahl, M. D., and Morris, P. J., "Noise from Supersonic Coaxial Jets, Part 1: Mean Flow Predictions," *Journal of Sound and Vibration*, Vol. 200, No. 5, 1997, pp. 643–663.

[8]Papamoschou, D., "Pylon-Based Jet Noise Suppressors," AIAA Paper 2008-0040, Jan. 2008.

[9]Brooks, T.F., and Humphreys, W.M., "A Deconvolution Approach for the Mapping of Acoustic Sources (DAMAS) Determined from Phased Microphone Arrays," *Journal of Sound and Vibration*, Volume 294, Issue 4-5, pp. 856-879.

[10]Papamoschou, D., "Imaging of Distributed Directional Noise Sources," AIAA Paper 2008-2885, May 2008.

Table 1. Flow conditions.

	Acoustic Tests	Pitot Surveys
U_p (m/s)	600	319
M_p	1.03	1.03
NPR_p	2.00	1.96
U_s (m/s)	400	213
M_s	1.15	0.65
NPR_s	2.25	1.33
A_s/A_p	1.40	1.40
U_s/U_p	0.67	0.67

Table 2. Deflector configurations and sample results.

	Vanes			Wedges		Downward results		Sideline results	
Case	Airfoil	φ_1 (deg)	φ_2 (deg)	Solidity	x_{apex} (mm)	$\mathcal{V}_{SC}/\mathcal{V}_{PC}$	ΔSPL (dB)	$\mathcal{V}_{SC}/\mathcal{V}_{PC}$	ΔSPL (dB)
Base	-	-	-	-	-	0.031	0.0	0.029	0.0
$2V_a$	4412	50	-	-	-	0.126	6.3	0.017	-0.3
$2V_b$	4412	90	-	-	-	0.099	7.0	0.068	0.3
$2V_c$	4412	120	-	-	-	0.061	4.1	0.106	4.5
$2V_d$	4412	150	-	-	-	0.044	2.4	0.040	2.8
$2V_e$	7514	90	-	-	-	0.072	6.1	0.062	3.7
$2V_e$	7514	120	-	-	-	0.046	4.7	0.064	6.5
$4V_a$	7514	50	120	-	-	0.210	7.7	0.040	6.6
$4V_b$	7514	90	120	-	-	0.148	8.4	0.040	3.7
$4V_c$	7514	90	150	-	-	0.094	8.1	0.070	3.9
$4V_d$	7514	50	90	-	-	0.156	9.5	0.024	1.9
W_a	-	-	-	0.5	0	0.049	3.4	0.053	3.1
W_b	-	-	-	1.0	0	0.040	5.5	0.071	2.5
W_c	-	-	-	0.5	4	0.037	5.8	0.037	2.8
W_d	-	-	-	1.0	4	0.040	4.3	0.036	3.3
W_e	-	-	-	0.5	8	0.040	3.3	0.037	3.0
W_f	-	-	-	1.0	8	0.039	6.2	0.039	3.3

All vanes had angle of attack of 4 deg, chord length of 3 mm and trailing edge located 2 mm upstream of the fan exit plane.
All wedges had half-angle of 20 deg, length of 10 mm, and transverse height of 4 mm
x_{apex}=axial distance of wedge apex from fan exit plane.
ΔSPL= Reduction in 18th 1/3-octave band level at θ=30 deg.

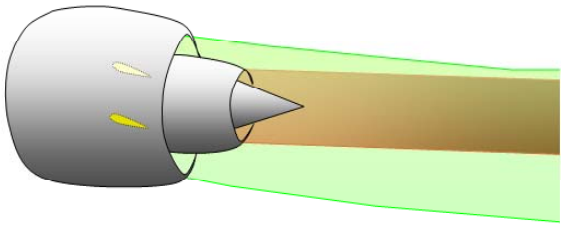

Fig. 1 General concept of fan flow deflection.

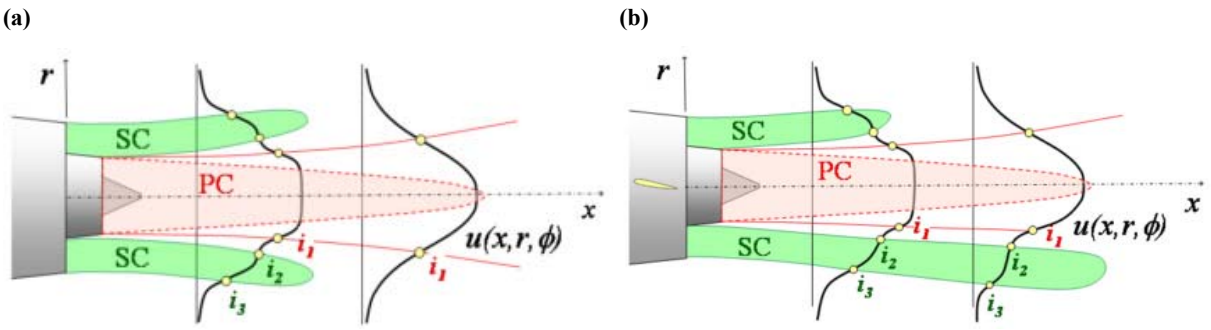

i_1,i_2,i_3=inflection points of radial velocity profile; PC=primary core, defined by a velocity threshold (e.g., $u/U_p \geq 0.8$); SC=secondary core, defined by the loop of inflection points *i2* and *i3*

Fig. 2 Deformation of the velocity profile from the coaxial state (a) to the distorted state (b) by the action of fan flow deflectors .

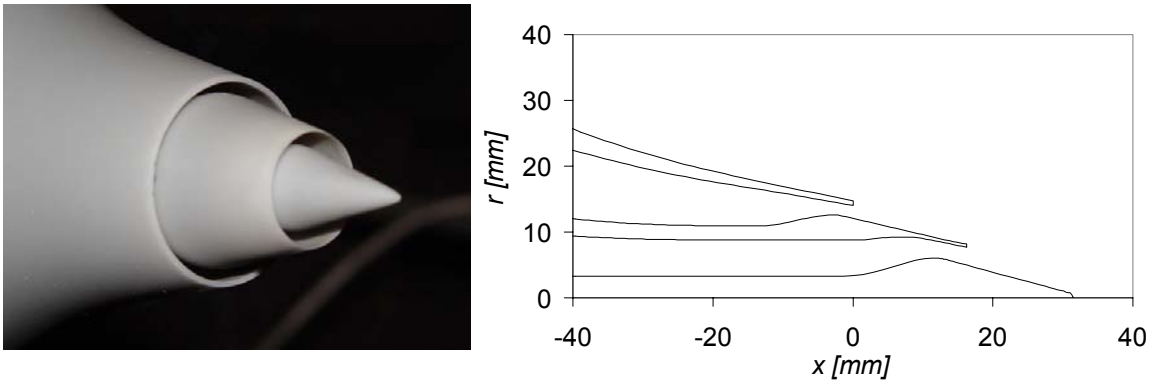

Fig. 3 Assembled nozzle and coordinates of the BPR = 2.7 nozzle.

Fig. 4 Types of deflectors used: (a) internal vanes; (b) external wedge.

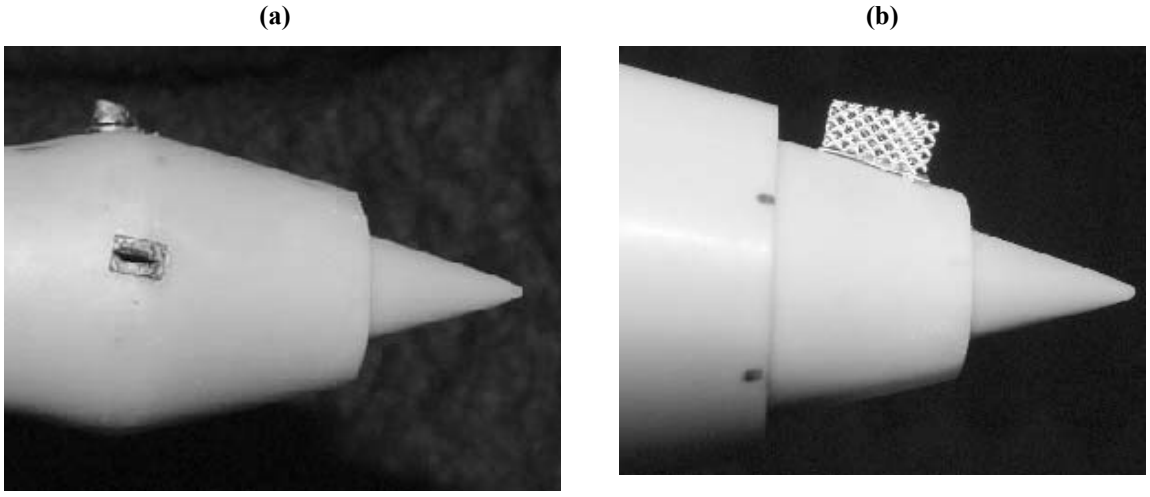

Fig. 5. Photos of some fan flow deflectors. (a) Example installation of vanes (shown without the fan duct); (b) perforated external wedge.

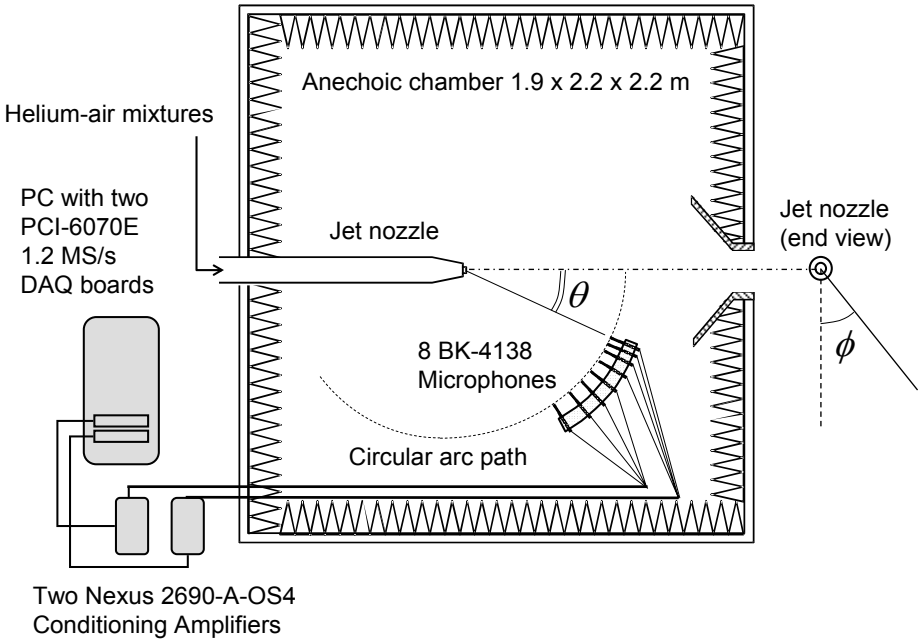

Fig. 6 Setup for aeroacoustic measurement.

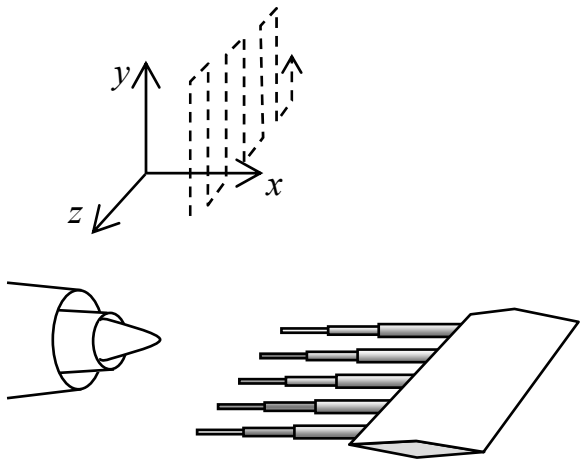

Fig. 7 Illustration of hypodermic-tip Pitot rake with nozzle and traverse path.

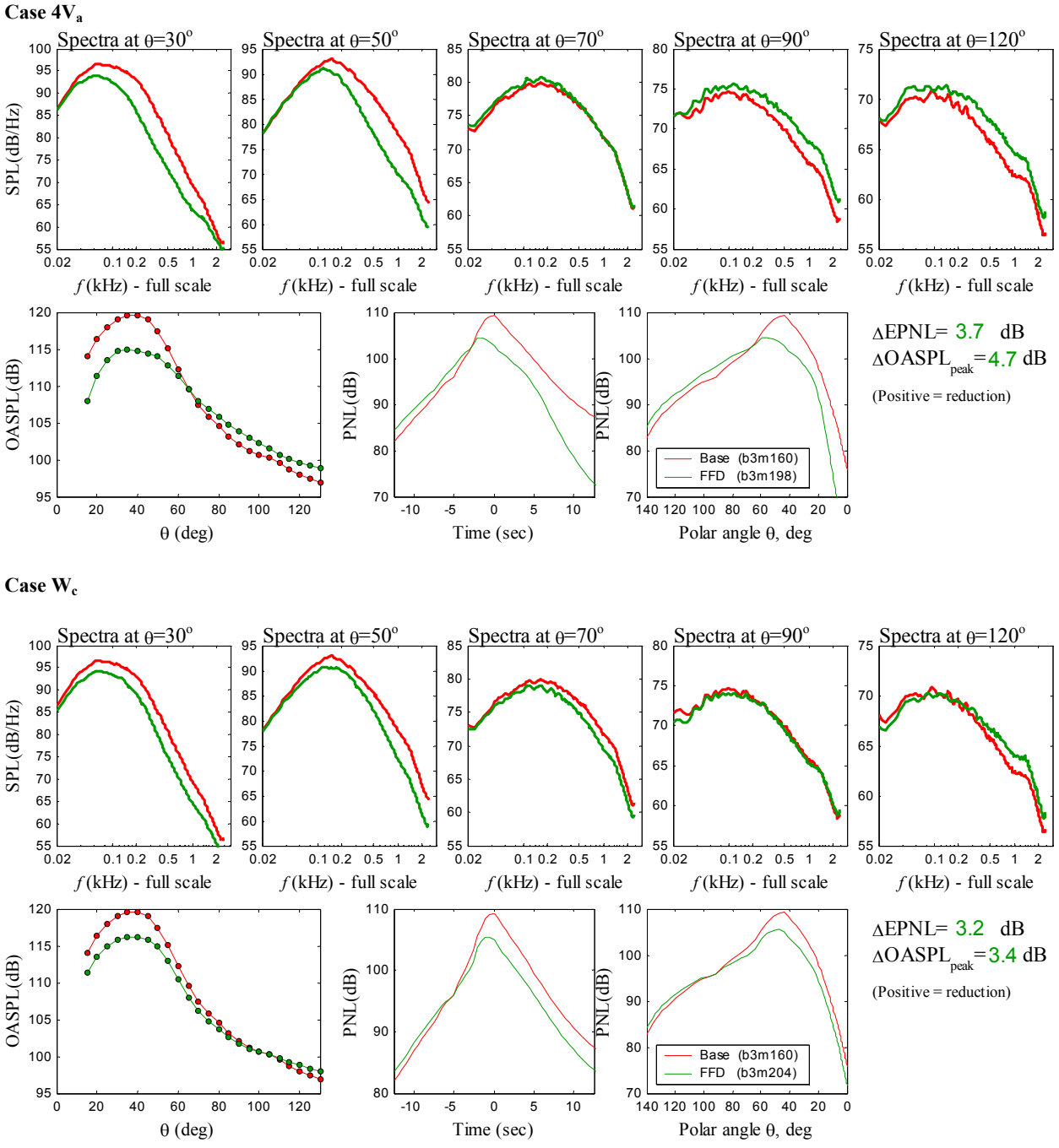

Fig. 8 Acoustic summary for $4V_a$ and W_c configurations with comparison to baseline. Microphone azimuth angle φ_{mic} = 0° (downward).

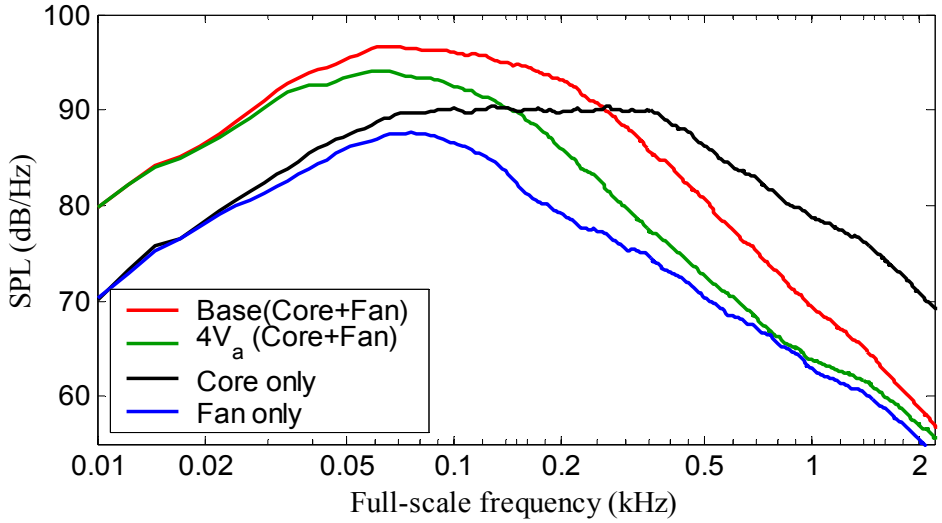

(a)

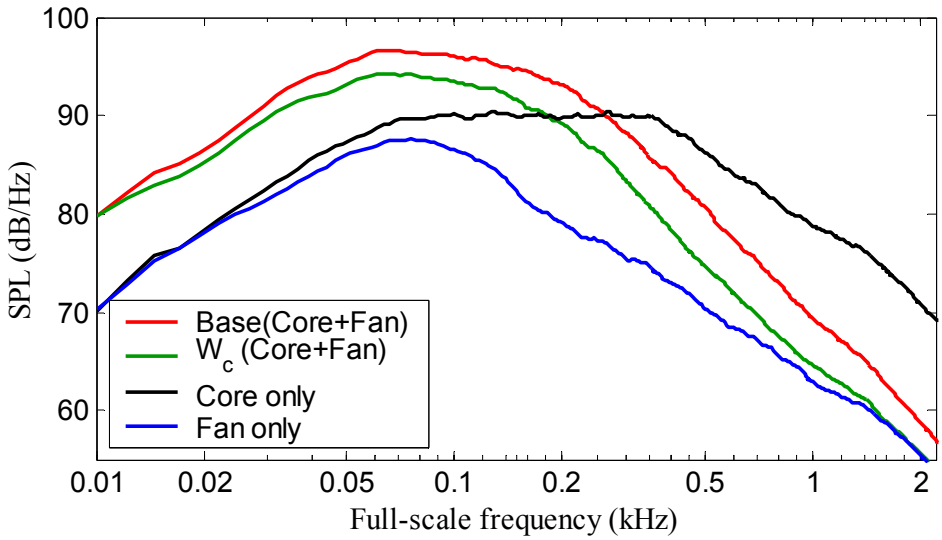

(b)

Fig. 9 Narrowband spectra at θ=30 deg, with comparison to core-alone and fan-alone cases. (a) $4V_a$; (b) W_c.

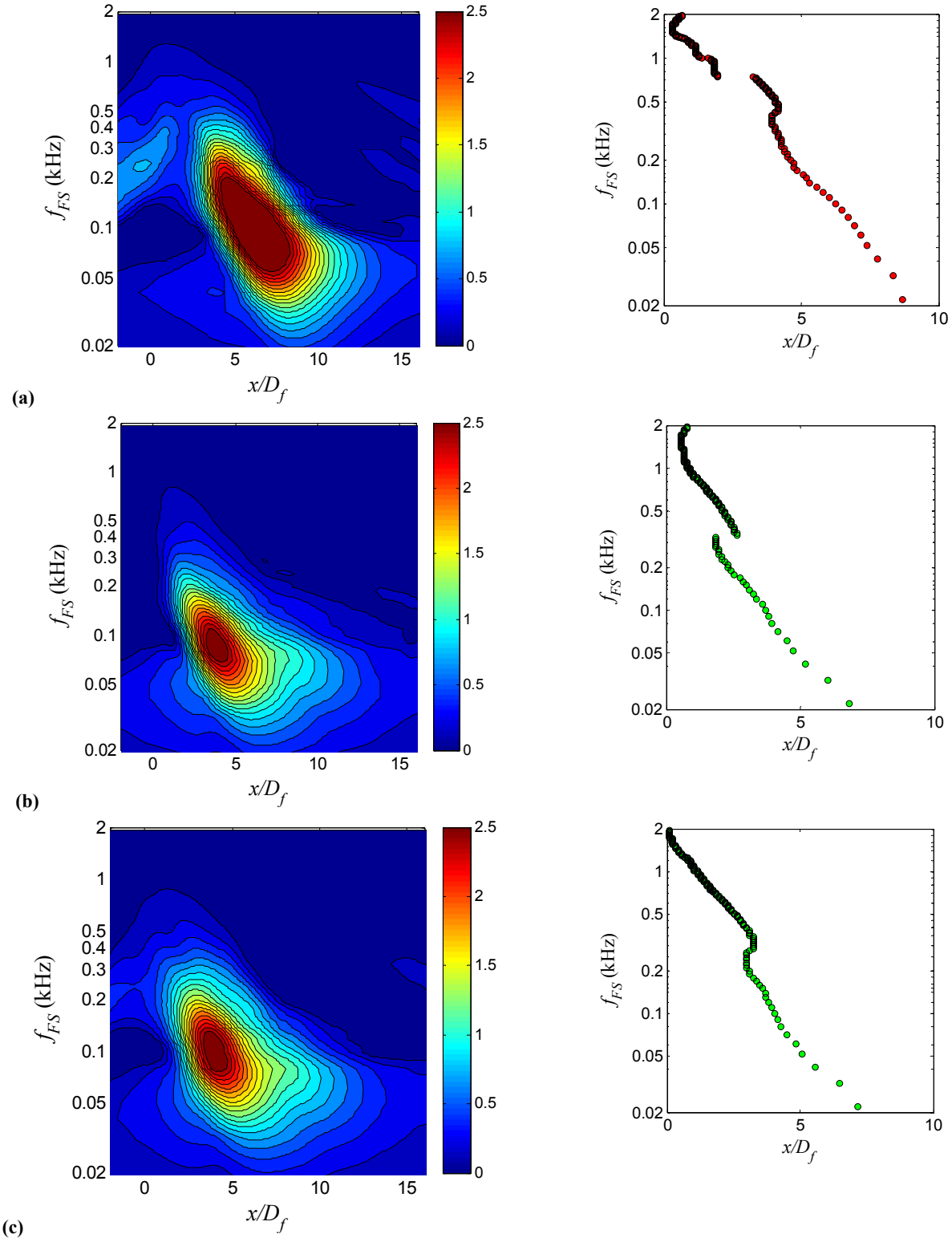

Fig. 10 Deconvolved noise source maps (left) and location of peak noise (right) in the direction peak emission for (a) baseline; (b) $4V_a$; (c) W_c.

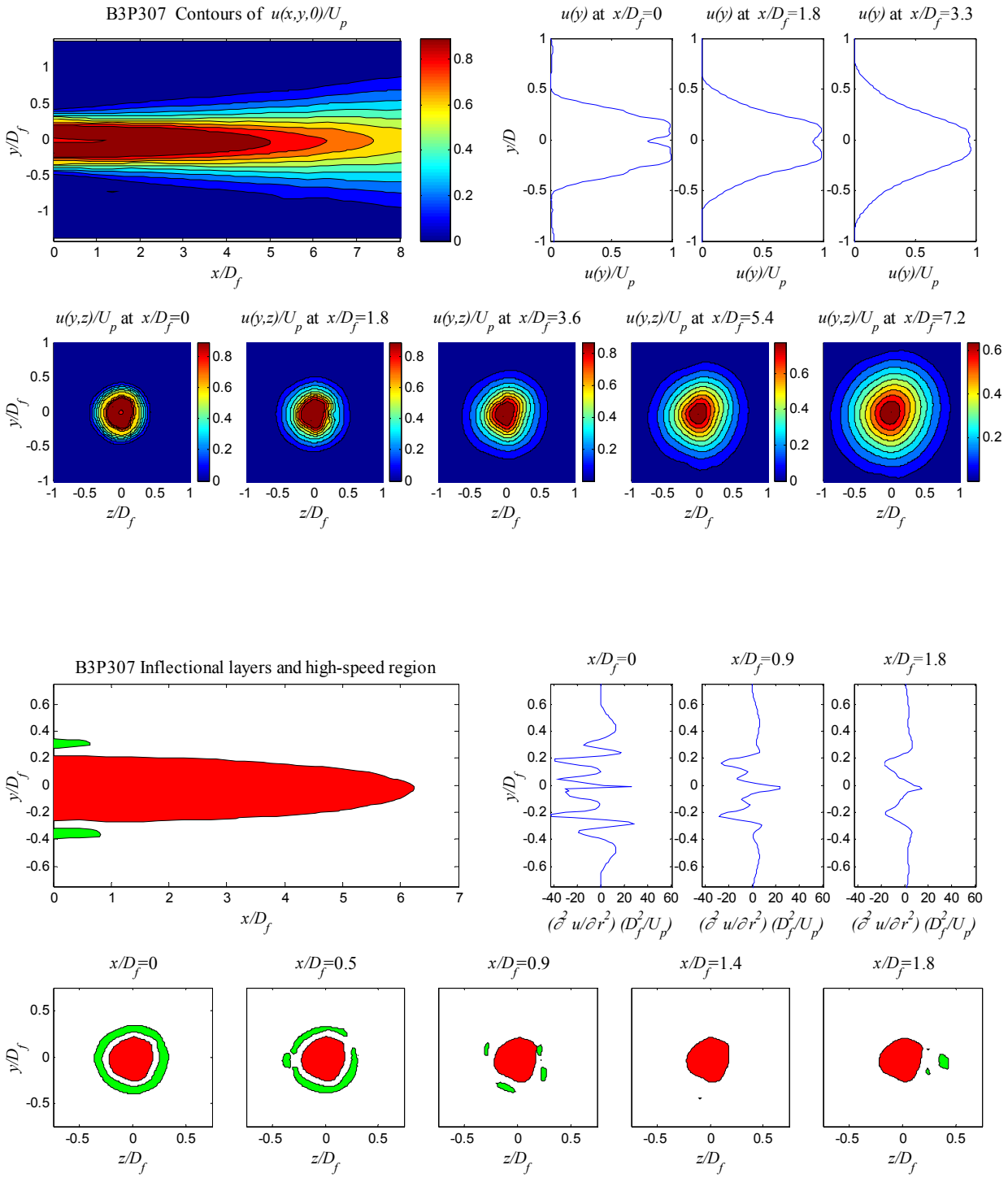

Fig. 11 Isocontours and line plots of velocity (top) and second radial derivative of velocity (bottom) for the baseline case. Bottom contour plots include extent of high-speed region $u/U_p > 0.8$.

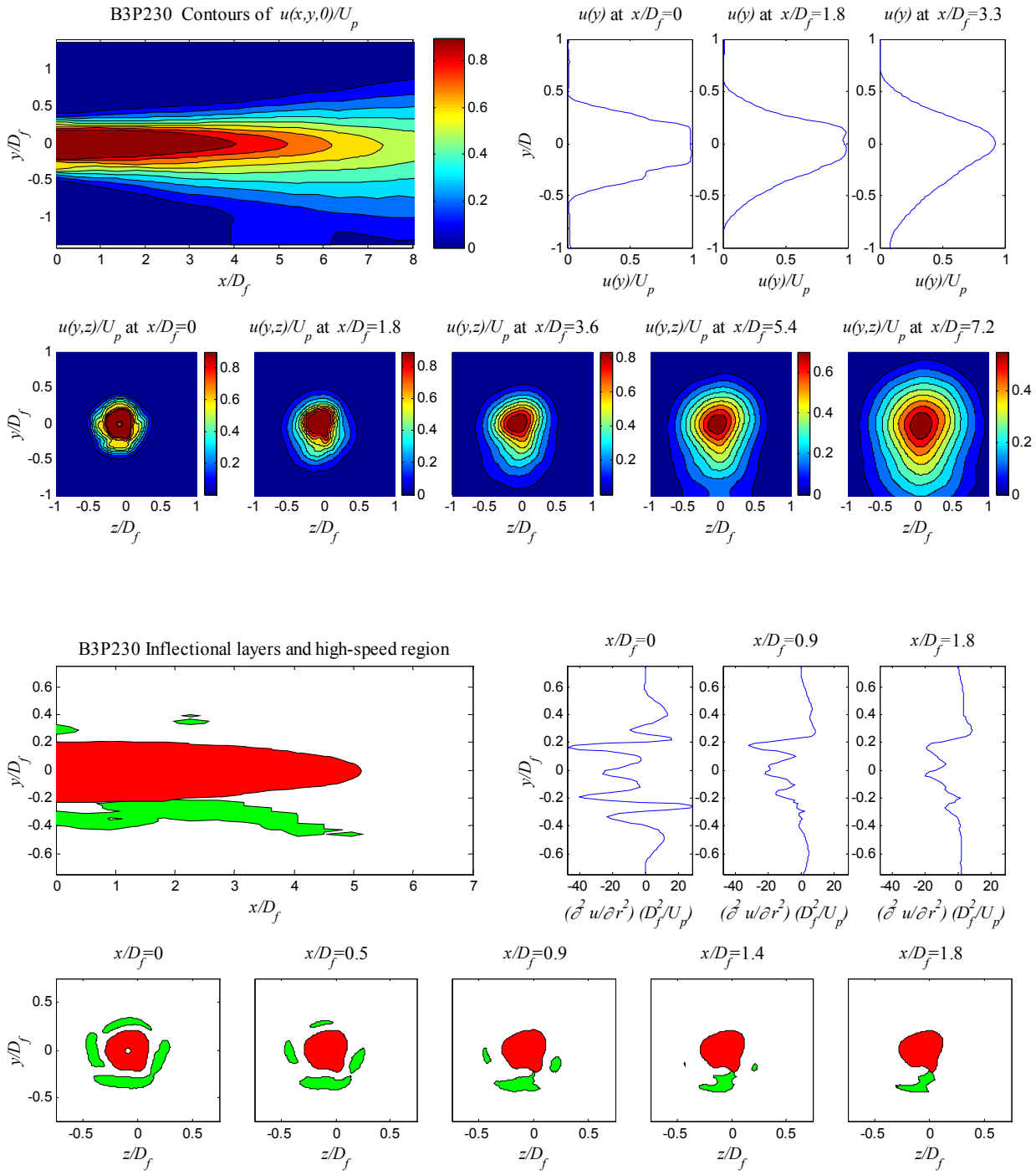

Fig. 12 Isocontours and line plots of velocity (top) and second radial derivative of velocity (bottom) for case 4Va. Bottom contour plots include extent of high-speed region $u/U_p > 0.8$.

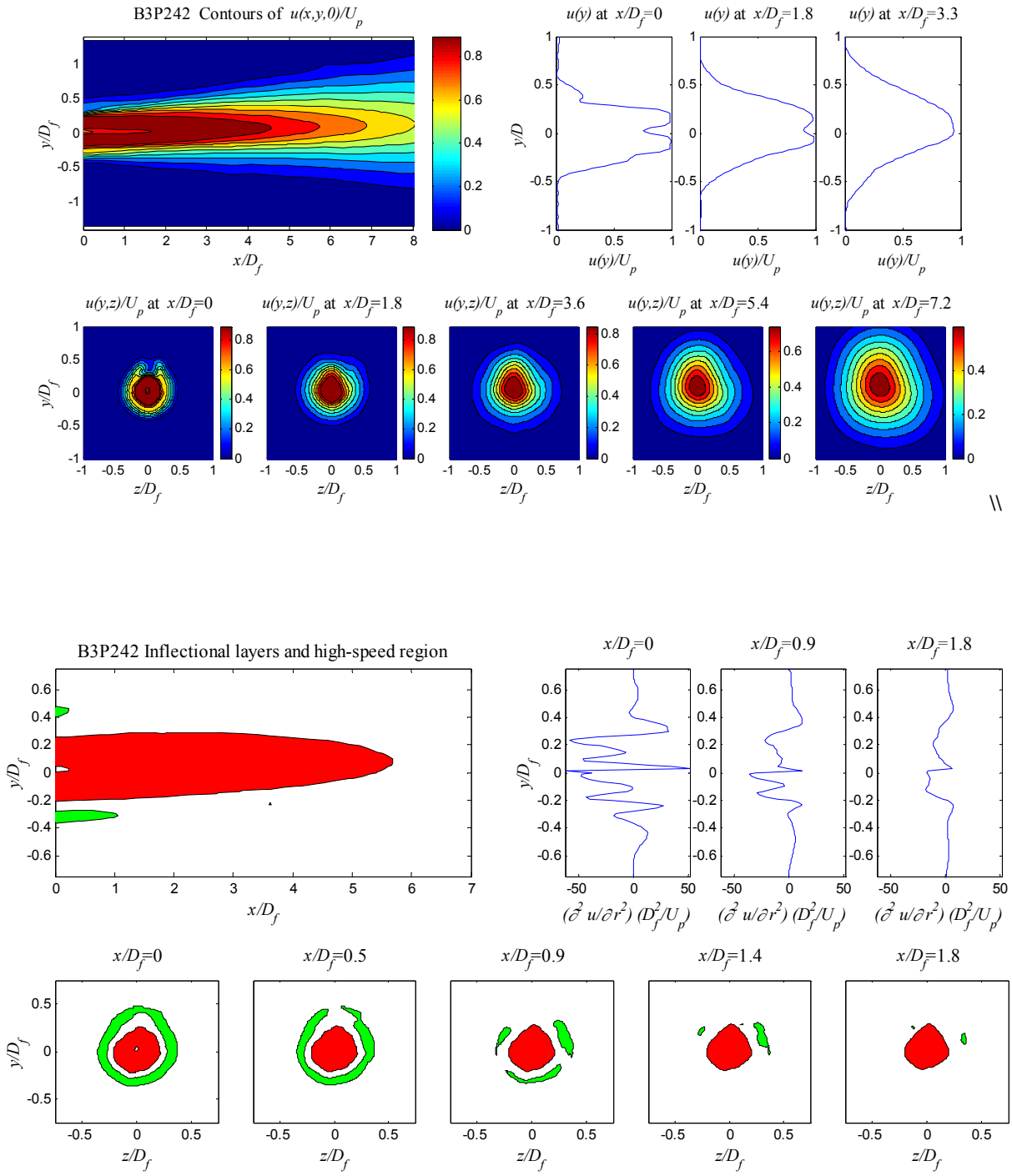

Fig. 13 Isocontours and line plots of velocity (top) and second radial derivative of velocity (bottom) for case W_c. Bottom contour plots include extent of high-speed region $u/U_p > 0.8$.

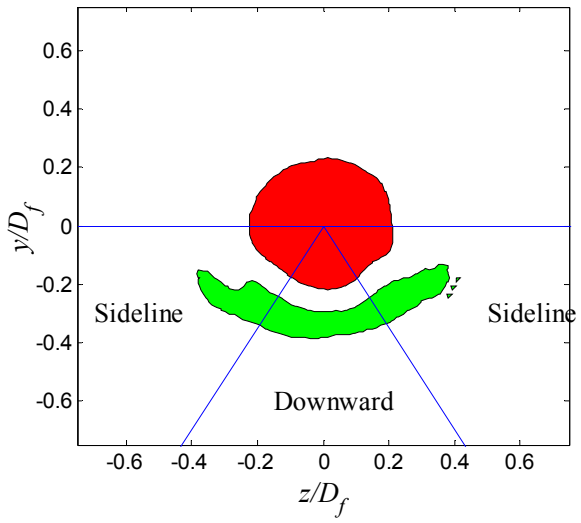

Fig. 14 High-speed region $u/U_p > 0.8$ (red) and inflectional layer (green) for case $2V_b$ at $x/D_f=1$. Division of inflectional area into downward and sideline components is illustrated.

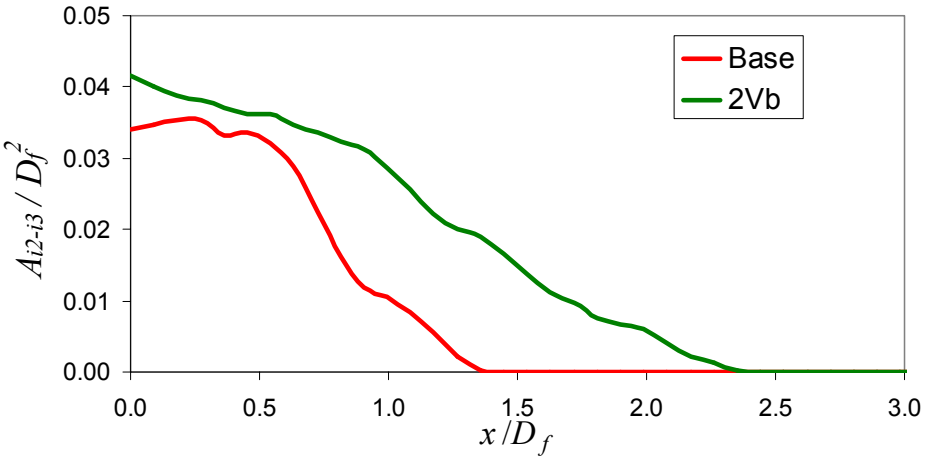

Fig. 15 Axial distribution of the area of the inflectional layer *i2-i3*, in the downward direction, for the baseline jet and jet $2V_b$.

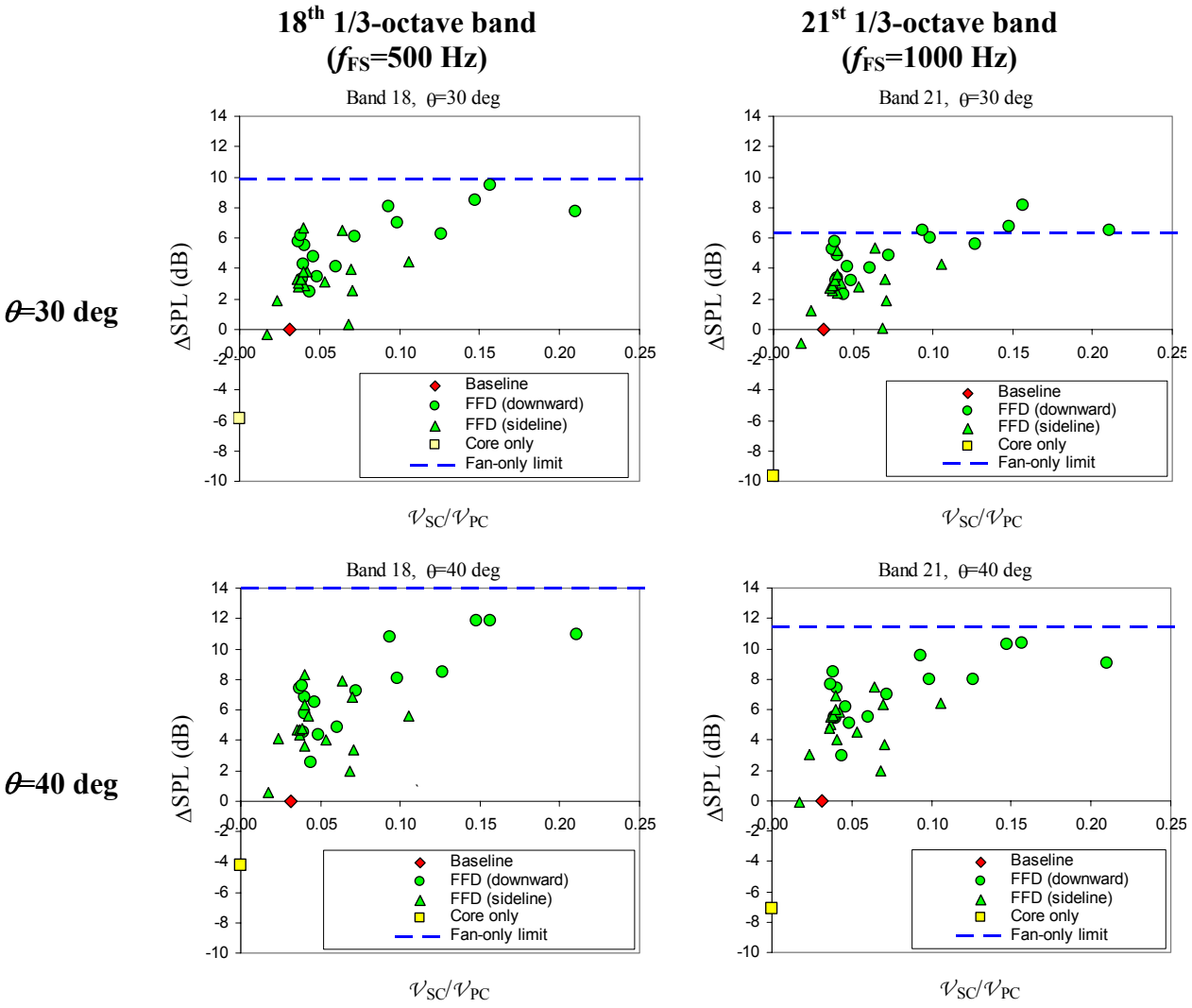

Fig. 16 Correlation of noise reduction relative to baseline versus volume of inflectional layers normalized by volume of high-speed region $u/U_p > 0.8$.